

The role of buoyancy in polarity reversals of the geodynamo

Binod Sreenivasan, Swarandeeep Sahoo and Gaurav Dhama

Centre for Earth Sciences, Indian Institute of Science, Bangalore 560 012, India. E-mail: bsreeni@ceas.iisc.ernet.in

Accepted 2014 September 2. Received 2014 September 1; in original form 2014 June 29

SUMMARY

We investigate polarity reversals in the geodynamo using a rotating, convection-driven dynamo model. As the flow in rapidly rotating convection is dominated by columns aligned with the axis of rotation, the focus is on the dynamics of columnar vortices. By studying the growth of a seed magnetic field to a stable axial dipole field, we show that the magnetic field acts in ways that significantly enhance the relative helicity between cyclonic and anticyclonic vortices. This flow asymmetry is the hallmark of a dipolar dynamo. Strong buoyancy, on the other hand, offsets the effect of the magnetic field, establishing parity between positive and negative vortices. As the dipole field is deprived of the helicity required to support itself, the dynamo is pushed into a reversing state. This is a likely regime for polarity reversals in the Earth's core. The integral lengthscale at which buoyancy injects energy is not significantly different from the convective flow lengthscale, which implies that buoyancy does not feed vortices at the small scales where non-linear inertia is present. The lengthscale at which the Lorentz force acts in the reversing dynamo is small, which may allow the passive presence of non-linear inertia in the small scales.

Key words: Numerical solutions; Dynamo: theories and simulations; Reversals: process, timescale, magnetostratigraphy; Planetary interiors.

1 INTRODUCTION

Geomagnetic reversals are perhaps the most interesting phenomena in geophysics. The dynamo operating in the Earth's outer core generates a predominantly north–south dipole magnetic field for long periods, but occasionally the magnetic dipole axis flips its orientation and retains its approximate alignment with the Earth's rotation axis. Although the current reversal frequency of the Earth's field is approximately 4 Myr^{-1} , the last reversal happened as long as 0.78 Ma and there have been long periods without recorded reversals, such as the Cretaceous Normal Superchron of 118–83 Ma. Excursions, the periods during which the dipole axis deviates considerably from the pole before returning to its original state, are more frequent in Earth's history. As reversals and excursions are likely to originate from similar convection states of the core (Gubbins 1999; Valet *et al.* 2005), it is possible that the geodynamo operates for long periods in a narrow transition zone that lies between dipolar and chaotic field configurations (Olson & Christensen 2006). In between, however, the dynamo might pass through relatively 'quiescent' periods of small secular variation that make the superchrons (McFadden & Merrill 1995).

Ever since the first polarity reversals were realized in numerical dynamo simulations (Glatzmaier & Roberts 1995a,b) several other studies have reported reversals in comparable parameter regimes (Sarson & Jones 1999; Wicht & Olson 2004; Aubert *et al.* 2008; Nishikawa & Kusano 2008; Olson *et al.* 2009, to name a few).

Diverse processes that take place during reversals have been identified, such as fluctuations in the meridional flow, formation of upwellings and breakdown of equatorial symmetry. There is, however, a broad agreement on two points: (i) Increasing the strength of the driving force pushes the dynamo from a stable dipole to a reversing regime (see, for example, Kutzner & Christensen 2002; Driscoll & Olson 2009); (ii) Reversals are 'kinematic' in the sense that the back reaction of the magnetic field on the flow appears to be small (see Sarson & Jones 1999; Wicht & Olson 2004; Rotvig 2009). As the second point above appears somewhat subtle, we shall re-examine the role of the magnetic field in the reversing dynamo, considering the local magnitudes of forces along columns parallel to the axis of rotation (z) which form in rapidly rotating convection.

An important issue that faces the dynamo theorist is whether polarity reversals in the geodynamo are caused by buoyancy-driven instabilities or by the dominance of non-linear inertia (that is, advection of momentum). Inertia is likely to play a role in several dynamo models because the parameters used are such that the Rossby number, $Ro = u/\Omega L$, which gives the ratio of inertial to Coriolis forces, is not small. (Here, u is the typical convective velocity, Ω is the background rotation rate and L is a length-scale of the order of the core depth.) Multipolar dynamos are obtained rather easily by operating at low values of the magnetic Prandtl number, Pm (Grote *et al.* 2000), upon which non-linear inertia enters the force balance by knocking out the magnetic Lorentz force in the Magnetic–Buoyancy–Coriolis (MAC) balance

(Sreenivasan & Jones 2006). Furthermore, the transition from dipolar to multipolar states happens when a local Rossby number, defined based on the lengthscale of convection rolls, takes on a value of ~ 0.1 (Olson & Christensen 2006), which suggests that inertia may not be small at the lengthscale of a fluid roll. It is not clear from simulations that reversals can happen in a strongly driven, yet low-inertia parameter regime (although this appears possible in Takahashi *et al.* 2005). In view of this, we investigate the role of inertia by looking at some typical lengthscales in the reversing and non-reversing regimes.

There is a significant body of literature that addresses the role of the lower mantle in controlling the frequency of polarity reversals (e.g. Glatzmaier *et al.* 1999; Kutzner & Christensen 2004; Olson & Amit 2014). Since compositional buoyancy is strong in present-day Earth, and the maximum variation in core–mantle boundary (CMB) heat flux is not likely to significantly exceed the mean heat flux through the core, the reversal process should have origins in buoyancy-driven instabilities in the core itself rather than in external heat flow variations. The lower mantle might have had a dominant role in producing reversals in early Earth when the core was largely thermally driven. In this paper, we do not look at the frequency of the reversals produced, but rather confine ourselves to the study of the reversal mechanism in strongly supercritical (thermochemical) convection that characterizes present-day Earth's core.

This paper stems from the idea that any explanation of polarity reversals must originate from an explanation of the preference for the axial dipole in rapidly rotating dynamos. Studies of rotating, convection-driven dynamos show that there is a large region of the parameter space where the axial dipole dominates (e.g. Katayama *et al.* 1999; Olson *et al.* 1999). The preference for axial dipoles is not simply a matter of having columns parallel to the rotation axis z with the right equatorial symmetry for the velocity. Rather, these coherent structures are affected by a pre-existing dipole magnetic field in ways that significantly enhance their helicity (Sreenivasan & Jones 2011); and since helicity is an important quantity for dynamo action (Moffatt 1978), the dipole field is preferred over other polarities. Whereas it is known that rotation via the Coriolis force acts as a source of vorticity (Chandrasekhar 1961), the magnetic field via the Lorentz force adds to the vortex stretching and a strong buoyancy force can potentially inhibit this process in ways that are yet to be understood. In this paper, we shall first test the hypothesis that the dipole magnetic field has self-generated helicity; we shall then address the polarity reversal problem by studying the effect of buoyancy on the dipole field.

2 NUMERICAL FORMULATION

We consider an electrically conducting fluid between two concentric, corotating spherical surfaces that correspond to the inner core boundary (ICB) and the CMB. The ratio of inner to outer radius is chosen to be 0.35. For simplicity, we assume that the fluid is subject to a thermal buoyancy-driven convection, although our set of equations can also be used to study thermochemical convection using the codensity formulation (Braginsky & Roberts 1995). The other body forces acting on the fluid are the Lorentz force, arising from the interaction between the induced electric currents and the magnetic fields and the Coriolis force originating from the background rotation of the system.

The governing equations considered are those in the usual Boussinesq approximation (Kono & Roberts 2002). Lengths are scaled by the thickness of the spherical shell L , and time is scaled by the mag-

netic diffusion time, L^2/η , where η is the magnetic diffusivity. The velocity field \mathbf{u} is scaled by η/L , the magnetic field \mathbf{B} is scaled by $(2\Omega\rho\mu\eta)^{1/2}$ where Ω is the rotation rate, ρ is the fluid density and μ is the magnetic permeability. The scaled magnetic field, known as the Elsasser number, Λ is an output derived from our dynamo simulations as a root mean square (rms) value, where the mean is a volume average.

The non-dimensional magnetohydrodynamic (MHD) equations for the velocity, magnetic field and temperature are

$$E P m^{-1} \left(\frac{\partial \mathbf{u}}{\partial t} + (\nabla \times \mathbf{u}) \times \mathbf{u} \right) + \hat{\mathbf{z}} \times \mathbf{u} = -\nabla p^* + Ra q T \mathbf{r} + (\nabla \times \mathbf{B}) \times \mathbf{B} + E \nabla^2 \mathbf{u}, \quad (1)$$

$$\frac{\partial \mathbf{B}}{\partial t} = \nabla \times (\mathbf{u} \times \mathbf{B}) + \nabla^2 \mathbf{B}, \quad (2)$$

$$\frac{\partial T}{\partial t} + (\mathbf{u} \cdot \nabla) T = P m P r^{-1} \nabla^2 T, \quad (3)$$

$$\nabla \cdot \mathbf{u} = \nabla \cdot \mathbf{B} = 0. \quad (4)$$

The dimensionless parameters in these equations are the Ekman number, $E = \nu/2\Omega L^2$ that measures the ratio of viscous to rotational forces, the Prandtl number, $Pr = \nu/\alpha$ that gives the ratio of viscous to thermal diffusivities, the magnetic Prandtl number, $Pm = \nu/\eta$ that gives the ratio of viscous to magnetic diffusivities and the Rayleigh number (see below). The Roberts number, $q = PmPr^{-1}$ is the ratio of thermal to magnetic diffusivities. The basic-state non-dimensional temperature profile represents a conventional basal heating, $T_b(r) = \beta/r$, where β is a constant. We set an isothermal condition at the ICB and a constant heat flux condition at the CMB. The modified Rayleigh number (the product of the classical Rayleigh number and the Ekman number) is based on the basic state heat flux, and is given by $Ra = g\gamma\beta/2\Omega\kappa$, where g is the gravitational acceleration acting radially inwards, γ is the coefficient of thermal expansion and κ is the thermal diffusivity. The velocity and magnetic fields satisfy the no-slip and electrically insulating conditions, respectively (Sreenivasan & Jones 2006). The Ekman number in our calculations is kept fixed at 3×10^{-4} , the Prandtl number is 1 and the magnetic Prandtl number is 5. These parameters were chosen so as to obtain polarity reversals at Rayleigh numbers that are large enough and yet achievable computationally.

3 RESULTS

3.1 Asymmetry induced by the magnetic field and its attenuation by buoyancy

We examine the role of buoyancy in the transition from a stable, dipole magnetic field state to a polarity flipping state by varying the Rayleigh number, Ra in steps in the range 200–1350 ($Ra/Ra_c \approx 5$ –33, where Ra_c is the critical Rayleigh number for onset of convection) while keeping the other parameters (Ekman number, Prandtl number and magnetic Prandtl number) fixed. Fig. 1 shows the magnetic colatitude of the dipole field, θ at the upper boundary (CMB) obtained from spherical-harmonic dipole coefficients, as follows:

$$\cos \theta = g_1^0 / |\mathbf{m}|; \quad \mathbf{m} = (g_1^0, g_1^1, h_1^1), \quad (5)$$

and

$$g_1^0 = \mathcal{P}_{10}, \quad g_1^1 = -2 \Re(\mathcal{P}_{11}), \quad h_1^1 = 2 \Im(\mathcal{P}_{11}), \quad (6)$$

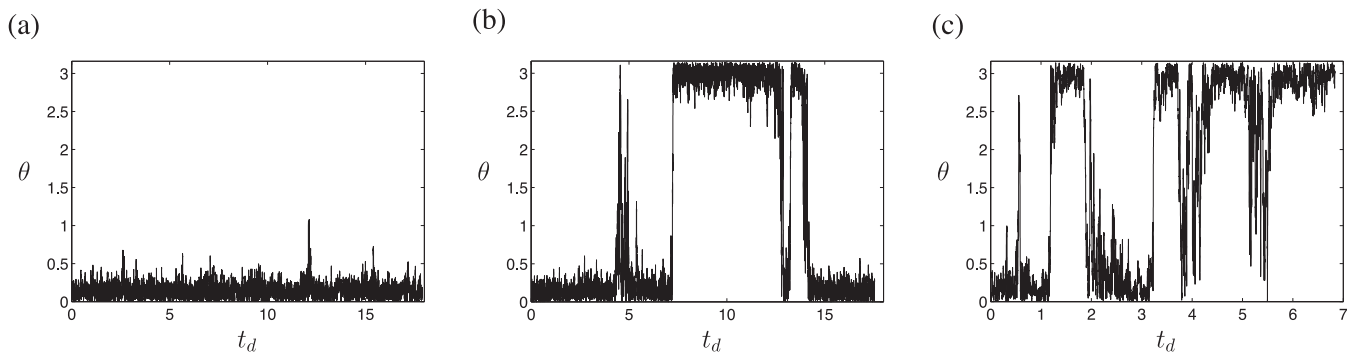


Figure 1. Dipole colatitude versus magnetic diffusion time for dynamo simulations at (a) $Ra = 810$, (b) $Ra = 990$ and (c) $Ra = 1350$.

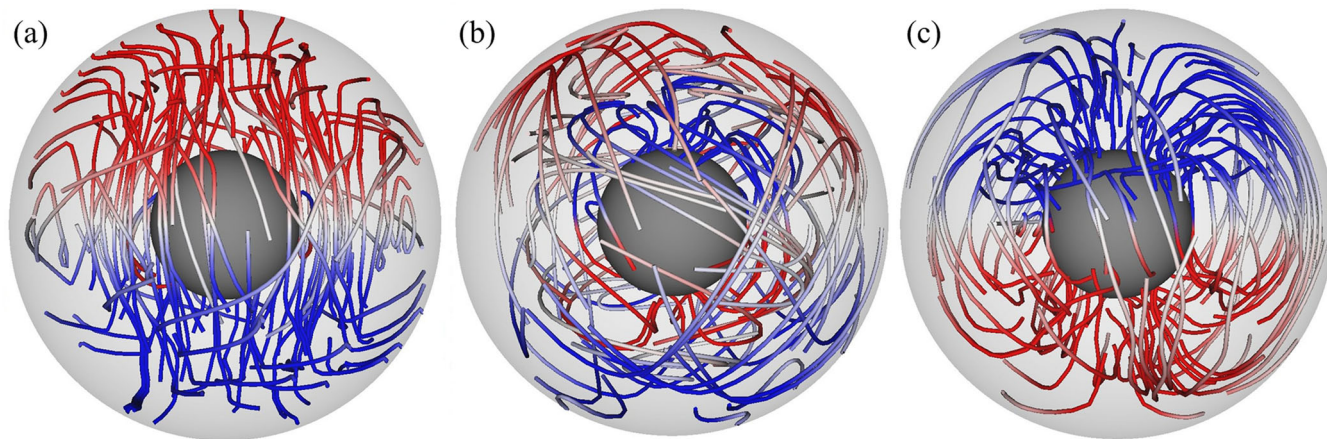


Figure 2. Streamlines of the Y_1^0 component of the magnetic field vector shown at three different snapshots in time during a polarity reversal at $Ra = 990$. The diffusion times are (a) 7.184; (b) 7.221; (c) 7.287.

where \mathcal{P} is the poloidal part of the magnetic field. Fig. 1 shows that the non-reversing axial dipole component is dominant for $Ra = 810$, whereas for $Ra = 990$, excursions and reversals of the dipole are present. The case $Ra = 1350$ is a chaotic, multipolar dynamo. The Y_1^0 component of \mathbf{B} for $Ra = 990$ is shown in Fig. 2 for three snapshots in time—at the start, during and at the end of a polarity reversal. The reversal period is ≈ 0.1 magnetic diffusion times, which is consistent with the estimate of a few thousand years for the core (Merrill & McFadden 1999; Dormy *et al.* 2000). The reverse flux originates in the Northern and Southern tangent cylinder region and grows to fill the entire hemisphere, somewhat similar to what was noted in some previous reversal simulations (Wicht & Olson 2004).

As one of the aims of this study is to understand the transition in dynamic behaviour as the dynamo enters a reversing regime, we begin the study with a run that produces a stable, non-reversing axial dipole. Fig. 3 shows the non-linear evolution in time of magnetic and kinetic energies for the run at $Ra = 300$ (Case 2, Table 2) starting from a seed magnetic field that has a dominant dipole component—that is, the radial and azimuthal components of the magnetic field are approximately antisymmetric about the equator. The magnetic field grows rapidly after about three magnetic diffusion times and saturates to a stable dipole field of Elsasser number ≈ 2.35 . The rise in magnetic energy is accompanied by a fall in the kinetic energy, signifying transfer of energy from the velocity field to the magnetic field by the Lorentz force. The growth of the magnetic field heralds a dramatic change in both magnitude and structure of the velocity field. In volume plots of isosurfaces of the axial velocity, u_z (Fig. 4), the positive (red) and negative (blue) values are shown

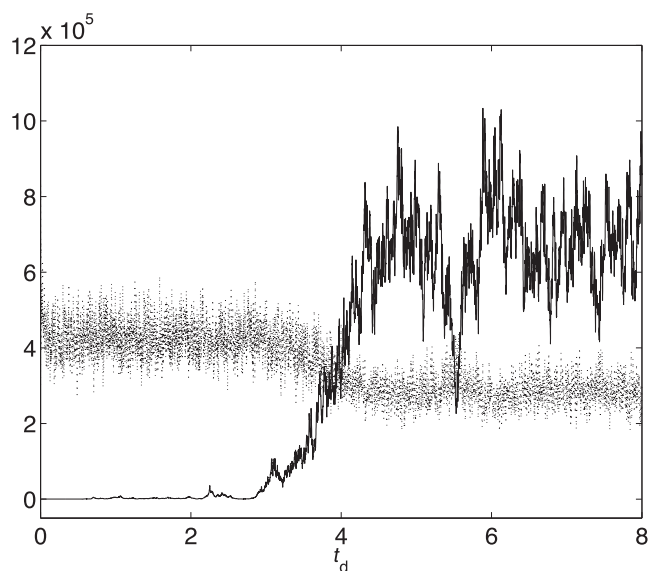


Figure 3. Evolution of kinetic energy (dotted line) and magnetic energy (solid line) with magnetic diffusion time for the dynamo simulation at $Ra = 300$, starting from a seed magnetic field.

separately for clarity. Figs 4(a) and (b) show a snapshot in the early (small-field) phase of the run ($t_d = 1.377$ in Fig. 3), where both positive and negative velocities are evenly distributed over the volume. The saturated phase in (c) and (d) ($t_d = 7.284$ in Fig. 3) shows a

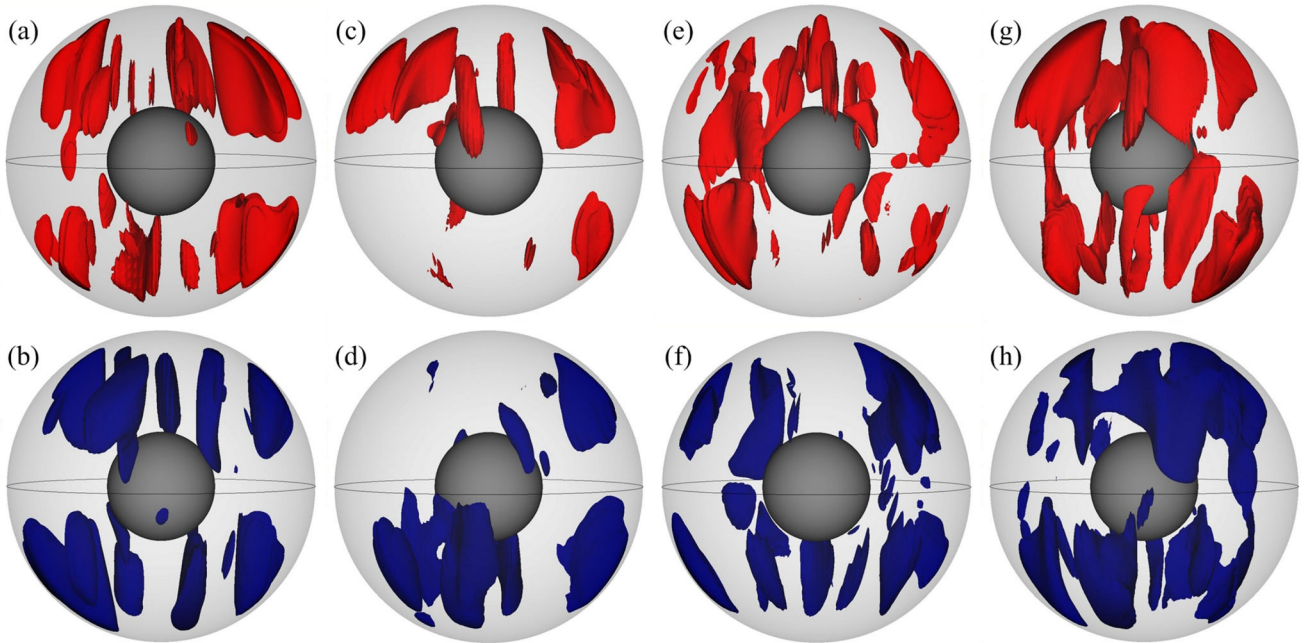


Figure 4. Volume plots of isosurfaces of the axial velocity, u_z , with positive values shown in red and negative values in blue. The snapshots shown (with values in brackets) are (a and b) $Ra = 300$, $t_d = 1.377 (\pm 220)$; (c and d) $Ra = 300$, $t_d = 7.284 (\pm 220)$; (e and f) $Ra = 630$, $t_d = 5.04 (\pm 300)$; (g and h) $Ra = 990$, $t_d = 2.47 (\pm 380)$. Also see Fig. 7 for the time-series at different Rayleigh numbers.

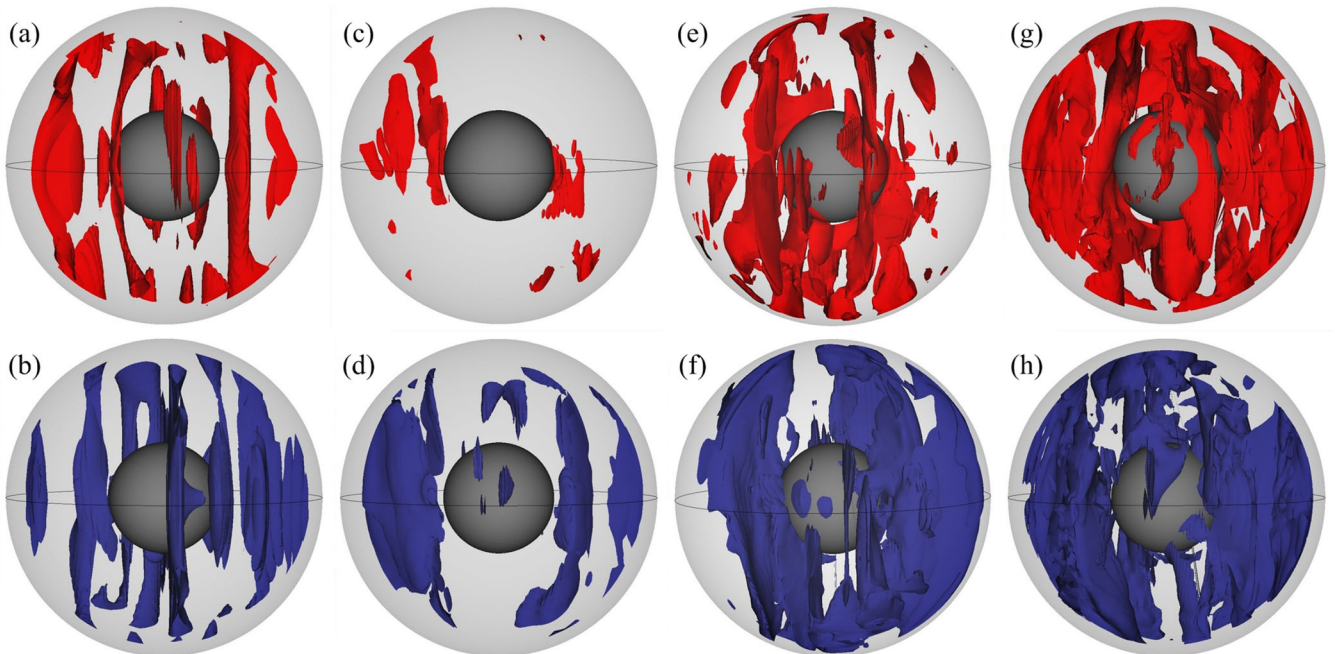


Figure 5. Isosurfaces of the axial vorticity, ω_z , with positive values shown in red and negative values in blue. The cases shown are (a and b) $Ra = 300$, $t_d = 1.377$; (c and d) $Ra = 300$, $t_d = 7.284$; (e and f) $Ra = 630$, $t_d = 5.04$; (g and h) $Ra = 990$, $t_d = 2.47$. The contour levels in each set of plots are ± 4000 .

marked asymmetry between the two signs of velocity. Positive velocities are favoured in the Northern (upper) hemisphere, whereas negative velocities dominate in the Southern (lower) hemisphere. A similar picture emerges for a broad range of contour levels. For small contour levels ($< \pm 100$), both positive and negative velocities are denser than in Figs 4(c) and (d), but the asymmetry between the signs exists. The flow asymmetry is not obvious at large contour levels, but their spatial distribution is too sparse to provide the physical picture that we seek. From Figs 4(e)–(h), we note that the asymme-

try between the two signs of velocity diminishes for $Ra = 630$, and is nearly absent for $Ra = 990$. The effect of the dipole magnetic field ($Ra = 300$) and the effect of increasing Rayleigh numbers ($Ra = 630, 990$) also show up in the distribution of axial vorticity, ω_z (Fig. 5). In the early phase of $Ra = 300$, both cyclones (positive ω_z , coloured red) and anticyclones (negative ω_z , coloured blue) are equally distributed (subfigures a and b, Fig. 5), whereas the saturated phase of the same run has a marked preference for anticyclonic vorticity (subfigures c and d, Fig. 5). As the Rayleigh

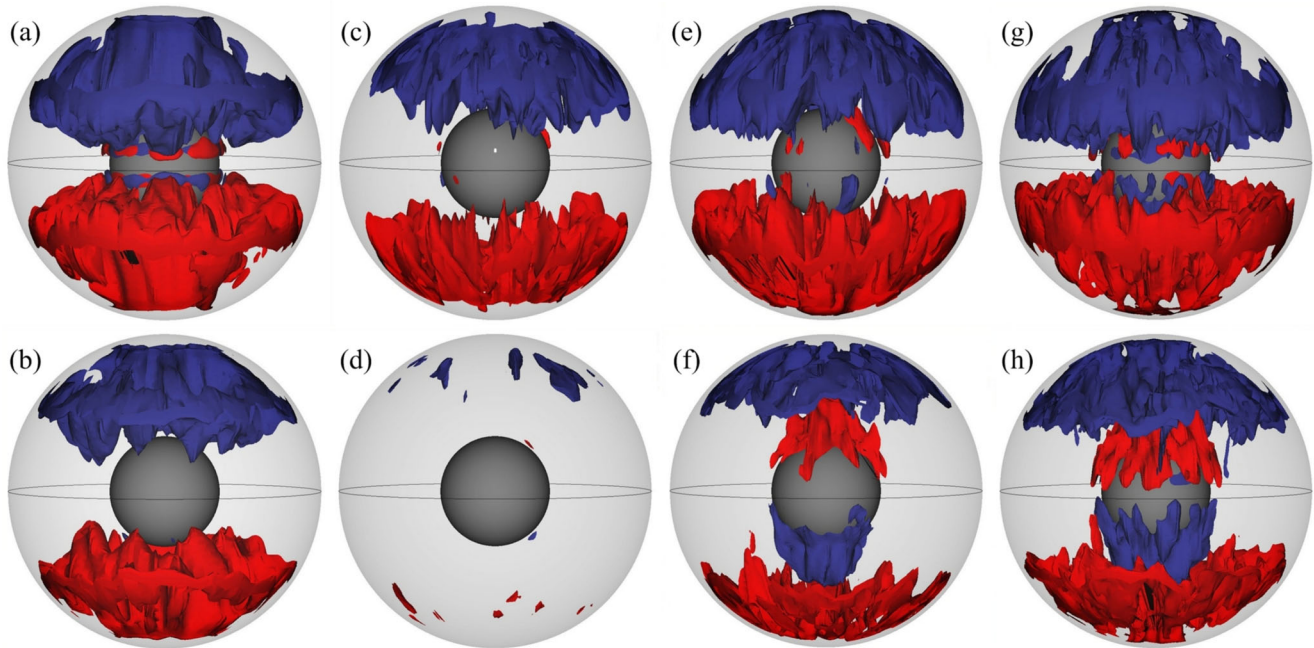


Figure 6. Time-averaged isosurfaces of the z -helicity, with anticyclonic helicity in the upper panel and cyclonic helicity in the lower panel. The contour levels shown are $\pm 2 \times 10^5$. Positive values are shown in red and negative values in blue. The cases shown are (a and b) $Ra = 300$ (non-magnetic); (c and d) $Ra = 300$ (saturated dipole); (e and f) $Ra = 630$; (g and h) $Ra = 990$.

number is increased to 630 and then 990, the skewness in vorticity gradually disappears (see e–h, Fig. 5). In effect, the magnetic field in the dynamo enhances axial fluid motion from the equator to higher latitudes, aiding the flow in anticyclones and negating the flow in cyclones. For moderate Rayleigh numbers, anticyclonic vorticity is dominant, whereas cyclonic vorticity is attenuated. For large Rayleigh numbers, the strong buoyancy appears to offset the asymmetry produced by the magnetic field.

Fig. 6(a–h) gives the time-averaged volumetric distribution of axial kinetic helicity ($u_z \omega_z$) contained in cyclones and anticyclones in separate panels. We consider the axial part of the scalar helicity because we are primarily interested in columnar fluid motion. For the ‘non-magnetic’ run at $Ra = 300$ (subfigures a and b, Fig. 6) we set the initial magnetic field to a very small value, so that the back reaction of the magnetic field on the flow remains small for at least eight magnetic diffusion times. For this run, both cyclonic and anticyclonic helicity are present in approximately equal measure. By contrast, in the saturated dipole regime of $Ra = 300$ the helicity is largely confined to the anticyclones (subfigures c and d, Fig. 6). This shows that the asymmetries in the velocity and vorticity are in phase, producing an amplified asymmetry in the helicity. Now, as the Rayleigh number is increased to 630 and 990 (subfigures e–h, Fig. 6), cyclonic helicity reappears, and eventually becomes dense, although the anticyclonic helicity is still dominant.

The line plots for the time evolution of axial kinetic energy density and helicity, shown in Fig. 7, support our findings so far: For the non-magnetic (that is, approximately kinematic) simulation at $Ra = 300$, the kinetic energies in cyclones and anticyclones almost overlap, and the same can be said of helicity (subplots a and b, Fig. 7). The initial phase of the dynamo simulation at $Ra = 300$ shows a similar behaviour, but the saturated phase is different in that the cyclones have lost more kinetic energy (and helicity) than the anticyclones (subplots c and d, Fig. 7). At higher Rayleigh numbers (630 and 990), the cyclones carry almost the same kinetic energy as the anticyclones, although the anticyclonic helicity is

still dominant in the reversing dynamo at $Ra = 990$ (subplots e–h, Fig. 7). In short, a non-reversing dipole exists in a regime where the magnetic field via the Lorentz force generates a preferred flow that supports the pre-existing field, whereas polarity reversals occur when the buoyancy force is large enough to offset the action of the magnetic field. In the next section, we shall see how buoyancy can overcome the preference for dipolar solutions even when the Lorentz force is significant.

To obtain a better feel for the distribution of energy and helicity in the dipolar and reversing regimes, we performed the following additional diagnostics for the upper (Northern) hemisphere, which are presented in Table 1:

- (1) A relative kinetic energy from ‘positive’ and ‘negative’ kinetic energy values:

$$E_R = \frac{E_{z+} - E_{z-}}{E_{z+} + E_{z-}}, \quad (7)$$

where $E_{z+} = \frac{1}{2} \int u_{z+}^2 dV$ is made up of only positive values of the velocity, and E_{z-} is made up of only negative values. For the non-magnetic simulation at $Ra = 300$, $E_R = 5.14$ per cent, whereas for the saturated dipole regime at $Ra = 300$, E_R is boosted to 22.76 per cent. In the reversing regime ($Ra = 990$), E_R falls to about 16 per cent.

- (2) The ratio of the ‘positive’ kinetic energy to the total kinetic energy, E_{z+}/E_z , in cyclonic and anticyclonic vortices. For the non-magnetic (NM) run at $Ra = 300$, the bulk of the energy in anticyclones is made up of positive (upward) velocity, whereas negative (downward) velocity dominates in the cyclones, consistent with the classical picture of non-magnetic convection (Olson *et al.* 1999). For the saturated dynamo at $Ra = 300$, E_{z+}/E_z in anticyclones has surprisingly not changed much, whereas in cyclones it has increased sharply from the non-magnetic state (Table 1). Since the equator-bound flow in cyclonic vortices is countered by the Lorentz force-driven flow, the vorticity skewness (subfigures c and d, Fig. 5) is due

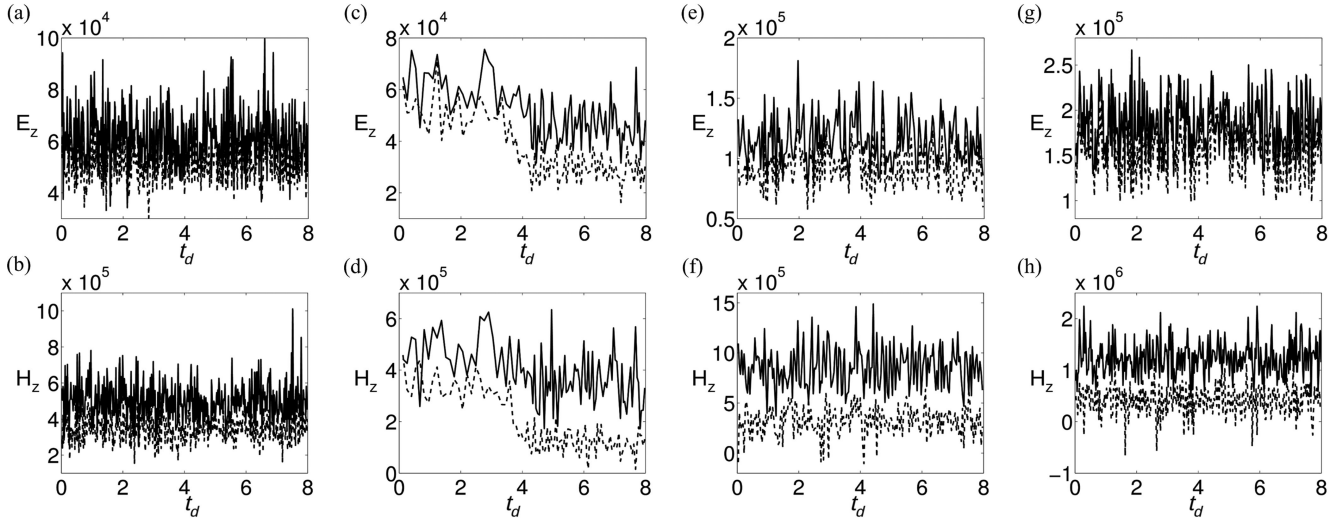


Figure 7. Upper panel figures show the total z -kinetic energy density, $\frac{1}{2} \int u_z^2 dV$ versus magnetic diffusion time, separately for anticyclones (solid lines) and cyclones (dashed lines). Lower panel figures show the total z -helicity, $\int u_z \omega_z dV$ for the lower hemisphere only, separately for anticyclones and cyclones. The cases shown are (a and b) $Ra = 300$ (non-magnetic); (c and d) $Ra = 300$ (dynamo evolution from seed field to saturated dipole); (e and f) $Ra = 630$; (g and h) $Ra = 990$.

Table 1. Summary of diagnostics performed for the upper (Northern) hemisphere. NM stands for non-magnetic, D stands for the saturated dynamo, A for anticyclones and C for cyclones. E_R is the relative z -kinetic energy density, defined by (7), E_{z+} is the z -kinetic energy calculated from positive z -velocity, E_z is the total z -kinetic energy and H_R is the relative helicity defined by (8).

	Ra (Run)	300 (NM)	300 (D)	630 (D)	900 (D)
1	E_R , per cent	5.14	22.76	16.86	15.88
2(a)	E_{z+}/E_z , per cent (A)	81.36	80.43	77.65	75.44
2(b)	E_{z+}/E_z , per cent (C)	18.41	31.43	34.04	37.57
3	H_R , per cent	17.89	48.69	45.33	44.62

to the compression of positive vorticity rather than the stretching of negative vorticity.

(3) A relative helicity, defined by

$$H_R = \frac{H_A - H_C}{H_A + H_C}, \quad (8)$$

where H is the volume integral of z -helicity and the subscripts A and C refer to anticyclones and cyclones. For the same Rayleigh number, the difference in H_R is large between strongly magnetic and non-magnetic states (Table 1). The growth in H_R is mainly due to a fall in the cyclonic helicity rather than a rise in the anticyclonic helicity (Figs 6 and 7); nevertheless, H_R is a useful measure of the helicity generated by the action of the magnetic field. As the Rayleigh number is increased, H_R decreases, but not significantly, showing that a modest reduction in H_R is enough to push the dynamo into a reversing regime.

3.2 Analysis of the vorticity equation

On time and volume average, the curl of the momentum equation takes the form

$$\underbrace{\nabla \times (\nabla \times \mathbf{B}) \times \mathbf{B}}_M + \underbrace{qRa \nabla \times (T\mathbf{r})}_A + \underbrace{\partial \mathbf{u} / \partial z}_C - \underbrace{EPm^{-1} \nabla \times (\boldsymbol{\omega} \times \mathbf{u})}_I + \underbrace{E\nabla^2 \boldsymbol{\omega}}_V = 0, \quad (9)$$

where $\boldsymbol{\omega} = \nabla \times \mathbf{u}$. Here, the letters M, A, C, I and V represent the Magnetic (Lorentz force), Archimedeian (buoyancy), Coriolis, non-linear Inertial and Viscous diffusion terms. Non-linear inertia is considered to be unimportant in the core because magnetic fields at the Rhines length scale (where inertia is important) will decay in less than a year (Sreenivasan & Jones 2006). In the next section, we examine whether non-linear inertia is likely to affect the reversal process. Due to the low Ekman number in the core, viscous diffusion would be small except in the Ekman layers at the top and bottom. In short, the geodynamo is likely to operate in an approximate balance between the MAC forces (Taylor 1963; Braginsky 1967). However, both inertial and viscous forces are certain to play a role in numerical dynamo models because it is not yet possible to solve the dynamo at realistic values of the Ekman number. Keeping in mind that our simulations at $E = 3 \times 10^{-4}$ are also likely to be affected by the artificial enhancement of inertial and viscous effects, we study the force balances in the non-reversing and reversing regimes, and the transition from one regime to the other. Fig. 8 gives the time-averaged, rms values of the terms in the vorticity equation as a function of the axial coordinate, z . Two cases are presented: $Ra = 300$ and 990. In subplots (a) and (c), all components are considered in evaluating the rms value, whereas in (b) and (d) attention is focused on the z -component, as we are particularly interested in columnar dynamics. The total rms plots show that the primary balance is between the Coriolis and buoyancy terms (the well-known thermal wind balance), except in the tangent cylinder region ($z > 1.44$). The inertial and viscous terms are much smaller than the Coriolis term, showing that the dynamo is in a rapidly rotating regime. For $Ra = 300$, the curl of the Lorentz force term is the third largest in magnitude for much of z , whereas at $Ra = 990$, this term is almost of the same order as the viscous and inertial terms. The z -rms plots in (b) and (d), on the other hand, show a markedly different behaviour: the dominant terms in the z -component of eq. (9) are the Coriolis (C) and the Magnetic (M) terms. This result is significant because it shows that the magnetic field has a strong effect on the columnar flow. For the non-reversing dipole state at $Ra = 300$, the M and C terms follow each other closely for almost all z ; for the reversing regime at $Ra = 990$, M can even locally exceed C. The A term expectedly decreases from the equator ($z = 0$)

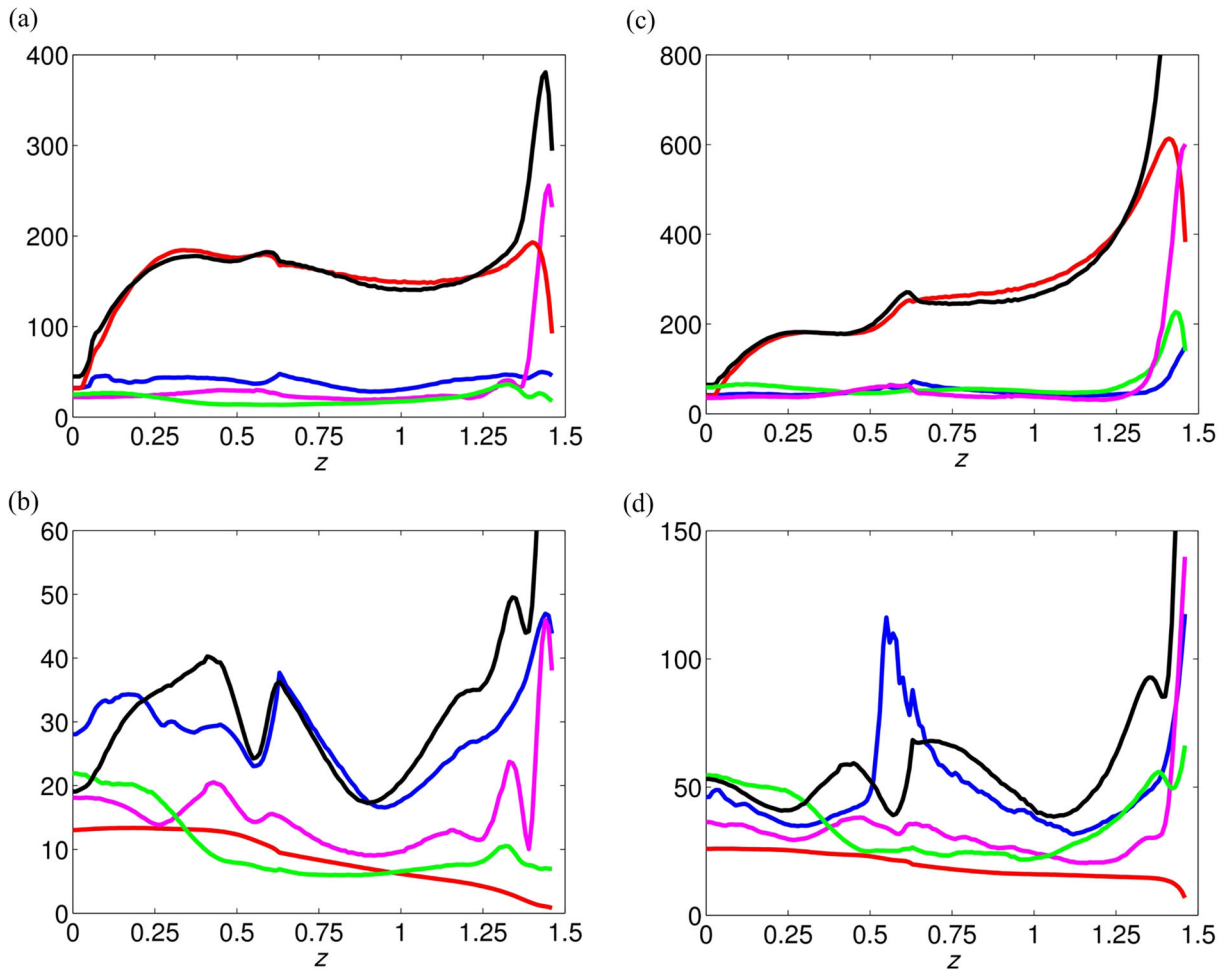


Figure 8. Upper panel figures give the time-averaged root mean square (rms) values of the terms in the vorticity equation as a function of the axial coordinate, z . Lower panel figures give the rms values of the z -component of the respective terms. The mean in rms is taken over the number of points at every z -section. The cases shown are (a and b) $Ra = 300$ (saturated dipole); (c and d) $Ra = 990$ (reversing). The terms plotted are magnetic, M (blue), buoyancy, A (red), Coriolis, C (black), non-linear inertia, I (green), viscous diffusion, V (magenta).

to the polar region and is smaller in magnitude than M and C. The I and V terms are not very small in the z -component, which means that they also enter the balance of terms in our model.

Fig. 9 gives the time-averaged MAC terms in the z -component of eq. (9) on a cylinder (z - ϕ plane) of radius $s = 1$, approximately midway between the cylinders that touch the ICB ($s = 0.538$) and CMB ($s = 1.538$). Analysis in cylindrical polar coordinates (s, ϕ, z) offers more insight than in spherical coordinates when we are concerned with columnar convection. Moreover, we ensure that the terms are not averaged over z or ϕ because we expect the dynamics in eq. (9) to be three-dimensional. The azimuthal structure of the solution does not disappear while averaging over several magnetic diffusion times because of the inherent flow asymmetry in the system. We first consider the stable dipole case at $Ra = 300$, where there is a strong correlation between the magnetic (M) and Coriolis (C) forces, as shown in Figs 9(a) and (c). For an axial dipole field, magnetic damping peaks not at the equator, but in regions above and below the equator, thereby producing coherent bands of positive $\partial u_z / \partial z$ between $z = 0$ and $z = \pm 0.5$. This important role of the magnetic field in stretching vorticity was predicted by Sreenivasan & Jones (2011) in their linear magnetoconvection model, wherein an azimuthal field with equatorial antisymmetry (that mimics an axial dipole) was imposed. The effect of magnetic friction is experienced

equally in cyclones and anticyclones, which would adequately explain the asymmetry in the columnar flow (subfigures c and d, Fig. 4), and the asymmetry in vorticity (subfigures c and d, Fig. 5). The back reaction of the magnetic field on the flow would be weak in a quadrupolar field configuration, wherein the driving buoyancy force and the damping magnetic force both peak at the equator. Unfortunately, it is not possible to study a quadrupolar field in our non-linear dynamo simulation because, irrespective of the structure of the starting seed field, the final field is always a dipole. (This point is not elaborated further as it will be the subject of a separate paper). We can, however, compare the saturated dipole state with the non-magnetic state at the same Rayleigh number (Fig. 10), in which case the curl of the buoyancy and Coriolis forces have neatly packed structures along the rotation axis.

It is clear from our simulations that, under rapid rotation, columnar vortices in convection are affected by the magnetic field in a way that increases their net helicity. An existing dipole field therefore holds itself up, which can explain why rotating dynamos should have a preference for north–south dipole fields. This also takes us to the central point of this paper—whether strong buoyancy can offset the effect of the magnetic field, causing collapse of the dipole. We find from our reversing simulation that this is indeed possible. In Fig. 9(d), the curl of the magnetic force is strong in

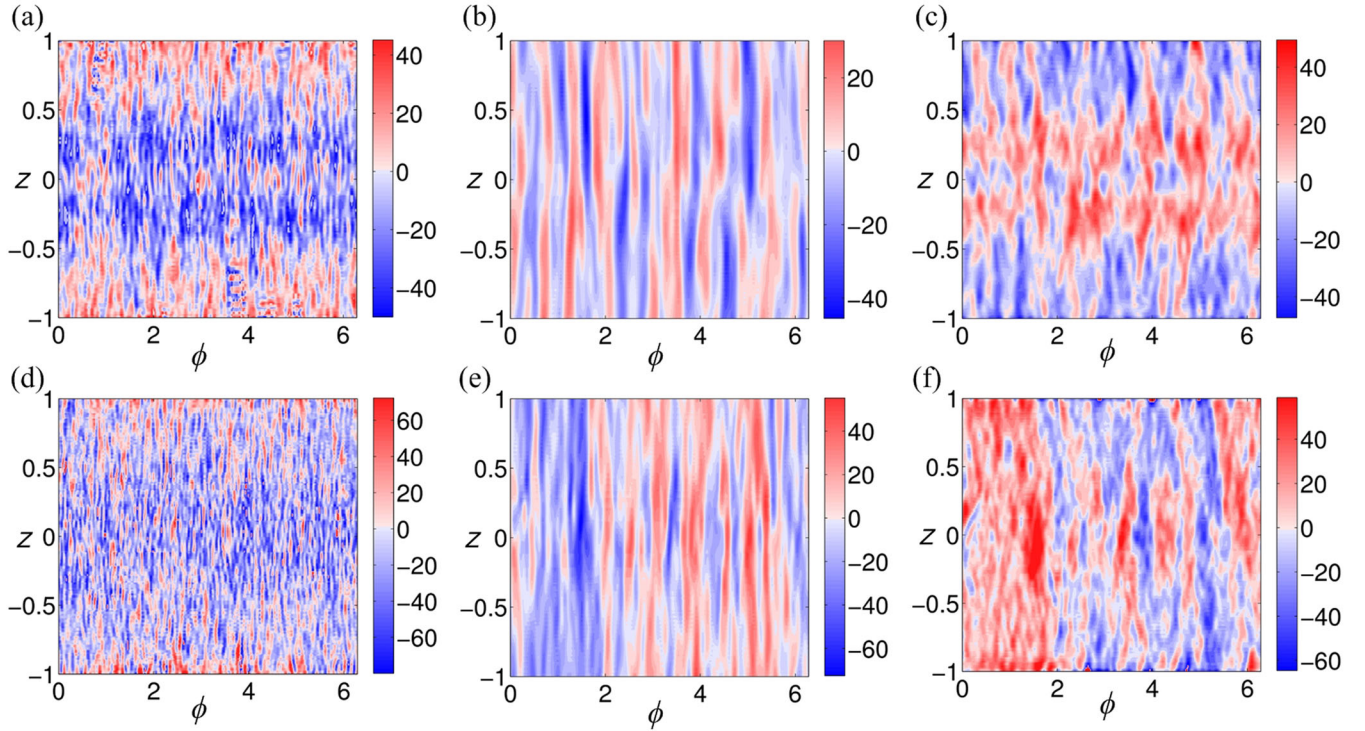


Figure 9. Contour plots of the time-averaged Magnetic (M), Archimedean (A) and Coriolis (C) terms in the z -vorticity equation, shown in that order, on a cylinder of radius $s = 1$. (a–c) Saturated dipole dynamo at $Ra = 300$. (d–f) Reversing dynamo at $Ra = 990$.

magnitude, but assumes a small-scale, scrambled structure that renders it ineffectual in changing $\partial u_z / \partial z$ through the Coriolis force. From the oppositely signed correlation between Figs 9(e) and (f) it is clear that the Coriolis force is largely controlled by buoyancy in this regime. (This effect would be missed in the azimuthal average as the z -component of the buoyancy term averages to zero.) The absence of a coherent $\partial u_z / \partial z$ implies that the asymmetry in the flow is significantly reduced; consequently the dynamo is deprived of the helicity required to support an axial dipole. However, how does buoyancy offset the magnetic feedback, when it is responsible for magnetic field generation in the first place? The answer to this question lies in the saturation mechanism of the dipole component of the field, which has not received much attention. Although the magnetic field is generated by induction, the M–C balance in the z -vorticity equation places an upper bound on the strength of the dipole component; so driving the dynamo harder only produces field components of other (non-dipolar) symmetry. The dynamo Elsasser numbers given in Table 2 seem to support this line of thought—for $Ra \geq 990$, the rise in Elsasser number likely results from the growth of non-dipolar field harmonics, unconstrained by rotation.

3.3 Lengthscales in the dynamo and the role of non-linear inertia in reversals

If the convective rolls in rotation have extent $\sim L$ parallel to the rotation axis and a shorter lengthscale, ℓ_c perpendicular to $\boldsymbol{\Omega}$, the non-linear inertia and Coriolis terms in the vorticity equation give the following order-of-magnitude estimates:

$$|\nabla \times (\nabla \times \mathbf{u} \times \mathbf{u})| \sim \frac{u_*^2}{\ell_c^2}, \quad |(\boldsymbol{\Omega} \cdot \nabla)\mathbf{u}| \sim \frac{\Omega u_*}{L}. \quad (10)$$

A balance between these two forces in the curl gives a very small value for $\ell_c \sim 4$ km, using $u_* \sim 4 \times 10^{-4}$ (Starchenko & Jones 2002). Motions on this lengthscale are not relevant to the geodynamo process because the magnetic fields generated on this scale would simply diffuse away on a short timescale of less than a year, assuming a magnetic diffusivity of $2 \text{ m}^2 \text{ s}^{-1}$. Even if non-linear inertia is only ~ 5 per cent of the Coriolis force, the lengthscale ℓ_c is ~ 15 km (~ 0.007 in dimensionless length units), which is unlikely to be sustained in the core, and unrealizable in numerical dynamo models. However, inertia can exist in the core if buoyancy continually replenishes vortices that are damped by the magnetic field. To examine this possibility, we calculate the typical lengthscale at which energy is injected by buoyancy, ℓ_E as a weighted average from the l -spectrum of $u_r T$, where u_r is the radial velocity and T is the temperature:

$$\frac{1}{\ell_E} = \frac{1}{\pi} \frac{\sum_l l E_T(l)}{\sum_l E_T(l)}. \quad (11)$$

The spectrum $E_T(l)$ is obtained from the product of the transform of $u_r T$ and its conjugate. The values of ℓ_E given in Table 2 suggest that injection of energy takes place at a lengthscale that is marginally smaller than the convective flow lengthscale, ℓ_c calculated from the kinetic energy spectrum (Table 2):

$$\frac{1}{\ell_c} = \frac{1}{\pi} \frac{\sum_l l E_k(l)}{\sum_l E_k(l)}. \quad (12)$$

In other words, lengthscales at which non-linear inertia is important are not likely to be fed by buoyancy.

A plausible way by which non-linear inertia can find its place in a reversing dynamo is through a small-scale balance with the Lorentz force term (M) in eq. (9). The typical lengthscale of the magnetic

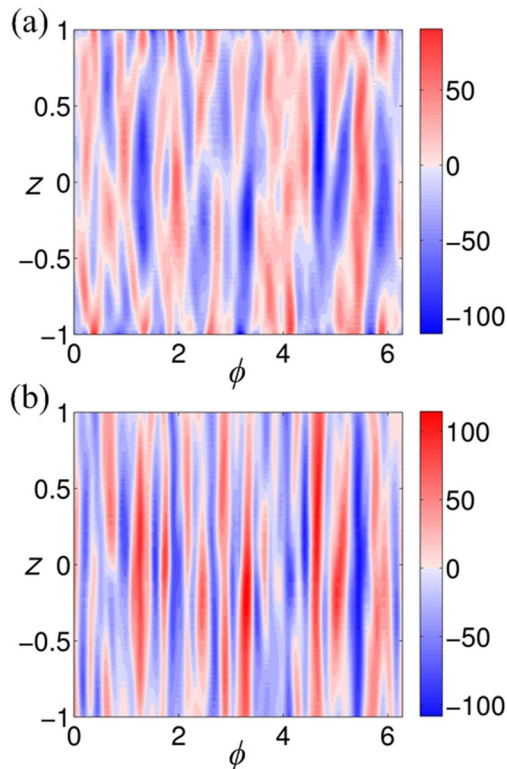


Figure 10. Contour plots for the non-magnetic simulation at $Ra = 300$ of (a) Buoyancy (A) and (b) Coriolis (C) terms in the z -vorticity equation. The plots are time-averaged and shown on a cylinder of radius $s = 1$.

Table 2. Summary of the dynamo runs performed, with lengthscale diagnostics. The parameters used in our models are $E = 3 \times 10^{-4}$, $Pr = 1$ and $Pm = 5$. Here Ra is the modified Rayleigh number, Rm is the magnetic Reynolds number, Λ is the Elsasser number derived from the saturated magnetic energy in the model, ℓ_c is the typical lengthscale of a convection roll, ℓ_E is the lengthscale at which energy is injected by buoyancy, ℓ_b is the magnetic field lengthscale and ℓ_O and ℓ_V are the Ohmic and viscous dissipation lengthscales.

Case	Ra	Rm	Λ	ℓ_c	ℓ_E	ℓ_b	ℓ_O	ℓ_V
1	200	152	2.31	0.431	0.345	0.432	0.219	0.284
2	300	196	2.35	0.378	0.295	0.341	0.182	0.251
3	630	305	2.33	0.332	0.261	0.235	0.132	0.225
4	810	353	2.36	0.334	0.258	0.210	0.123	0.220
5	990	394	2.50	0.336	0.256	0.200	0.119	0.217
6	1350	464	2.58	0.344	0.255	0.181	0.112	0.212

field, ℓ_b is obtained by from the magnetic energy spectrum, $E_m(l)$ by the same procedure as in (12). Furthermore, the Ohmic dissipation lengthscale, ℓ_O is obtained from the dissipation spectrum, $D_m(l)$ which is made up of the harmonic distribution of $(\nabla \times \mathbf{B})^2$. Both ℓ_b and ℓ_O decrease with increasing Rayleigh number (Table 2), which suggests that, in the reversing dynamo the Lorentz force can be forced to operate at the small scales where inertia also exists. Fig. 11 shows that the inertial term, I for both $Ra = 300$ and $Ra = 990$ has a small-scale, scrambled structure. The comparison with M in Fig. 9(d) shows that M and I have comparable structures for $Ra = 990$, whereas for the stable dipole at $Ra = 300$, the coherent, banded structure of M has no obvious correlation with I .

We must note that our reversing regime at $Ra = 990$ is fundamentally different from the multipolar, low- $Pr = Pm$ solution

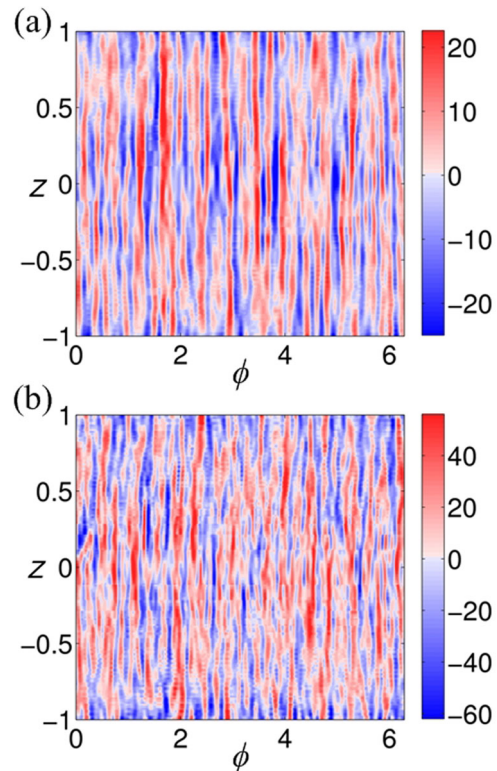


Figure 11. Contour plots of the time-averaged non-linear inertial (I) term in the z -vorticity equation, shown on a cylinder of radius $s = 1$. The cases presented are (a) $Ra = 300$ (saturated dipole dynamo); (b) $Ra = 990$ (reversing dynamo).

of Sreenivasan & Jones (2006): In their study, inertia was artificially boosted so as to disturb the MAC balance (and hence the axial dipole), whereas in this study, inertia owes its existence to the small-scale magnetic field in the reversing dynamo.

We conclude our discussion on lengthscales by noting that the energy injection scale, ℓ_E is greater than the Ohmic dissipation scale ℓ_O , implying a forward cascade of energy. However, viscous dissipation is marginally (a factor of 2 at $Ra = 990$) higher than Ohmic dissipation, and operates at a lengthscale, ℓ_V that is larger than that of Ohmic dissipation, ℓ_O (Table 2). This is essentially a consequence of the value of E and Pm used in the simulations, which makes the lengthscale of the convection rolls, ℓ_c of the same order of magnitude as, or even higher than, the magnetic field lengthscale, ℓ_b . In the core, we expect (i) a small-scale velocity field to give rise to a large-scale, mean magnetic field; and (ii) Ohmic dissipation to be the dominant means of energy decay. To realize this regime in a dynamo model, we require a separation of scales between the velocity and magnetic fields, made possible by a low-magnetic Prandtl number, Pm . Low- Pm dynamos require low E to operate, but produce magnetic fields that are strongly dipolar unless the Rayleigh number is set to a high value (Sreenivasan 2010); unfortunately, the low- E -high- Ra regime is very expensive computationally.

4 CONCLUSION

In a previous study, Sreenivasan & Jones (2011) showed via a linear magnetoconvection model in the limit of $E \rightarrow 0$ that a dipole magnetic field acting through the Lorentz force enhances helicity. The non-linear calculations of Sreenivasan & Jones were focused on the subcritical regime, wherein it was shown that a strong magnetic

field generates helical fluid motion in regions that are otherwise quiescent. This allows the operation of a strong-field dynamo at a Rayleigh number lower than that required for a seed field to grow. (Note, however, that the Rayleigh number is still above the critical value for onset of non-magnetic convection.) In this study, we verify the hypothesis of helicity generation by focusing on the dynamics of columnar vortices that form in a rapidly rotating dynamo. It is not clear whether helicity is important for magnetic field generation in any class of non-linear dynamos, but at least in rapidly rotating flows where first-order smoothing (Moffatt 1978) is applicable, helicity strongly affects dynamo action. Because of the dynamic, self-generated magnetic field, dynamo simulations are in general more difficult to interpret than linear magnetoconvection models; nevertheless, the evolution of a dynamo from a seed field provides the ideal test bed to look for changes in the flow that result from an increase in the magnetic field strength. Owing to the transfer of energy from the velocity to the magnetic field by the Lorentz force, the total kinetic energy (and helicity) in the dynamo decreases as the magnetic field grows, an effect not considered in the onset of linear magnetoconvection. So the effect of the dipole field is visible not in the total helicity, but in the difference between the helicity tagged to positively and negatively signed vortices (cyclones and anticyclones). The asymmetry in flow and vorticity brought about by the magnetic field (Figs 4 and 5) are in phase, resulting in an enhanced helicity in anticyclones relative to cyclones (Figs 6c and d and Table 1). From Table 1, we note that the decrease in relative helicity at high Rayleigh numbers is less dramatic than the increase in relative helicity of the magnetic state over non-magnetic convection. That is, the erosion of field-induced helicity by buoyancy is partial; therefore buoyancy does not push the dynamo back into a kinematic state.

An important result that has come out of this study is the large magnitude of the Lorentz force term (M) in the z -vorticity equation, in both dipole-dominated and reversing regimes (Figs 8b and d). This emphasizes the need to look at columnar dynamics in rapidly rotating dynamos. The Lorentz–Coriolis (M – C) force interaction in the z -vorticity equation is strong in the dipole-dominated regime ($Ra = 300$) and weak in the reversing regime ($Ra = 990$), which makes this equation an important starting point in the study of reversals. From a theoretical/numerical standpoint, it is worth investigating the saturation of the dipole component in the dynamo, and then the additional forcing required to dislodge the dipole by equilibrating the flows in cyclones and anticyclones. Through this approach, it may be possible to place bounds on the Rayleigh number for polarity reversals in the core.

Another important issue is whether geomagnetic field reversals are buoyancy-driven or inertia-driven. Our study strongly suggests that it is buoyancy that overcomes the preference for dipolar solutions by reducing flow asymmetries, and that non-linear inertia is not a participant in this process. Any presence of non-linear inertia in the small scales is likely to be a consequence of the small-scale magnetic structure produced in the reversing regime.

There is a compelling analogy between the action of the dipole magnetic field and the action of an equatorially symmetric CMB heterogeneity (Sreenivasan 2009). As both phenomena work through the z -vorticity equation, they produce similar effects—a rise in z -velocity, skewness in z -vorticity and consequent generation of helicity. Increasing the Rayleigh number swamps the effects of the dipole field (this study) as well as the CMB variations (Sreenivasan & Gubbins 2008). As the Earth's observed magnetic field is neither a perfect dipole nor a boundary-locked solution, there is hope that

dynamo models can eventually place bounds on the Rayleigh number of the core.

ACKNOWLEDGEMENTS

BS thanks the Department of Science and Technology (Government of India) for the award of a SwarnaJayanti Fellowship. We also thank the referees for their helpful comments.

REFERENCES

- Aubert, J., Aurnou, J. & Wicht, J., 2008. The magnetic structure of convection-driven numerical dynamos, *Geophys. J. Int.*, **172**, 945–956.
- Braginsky, S.I., 1967. Magnetic waves in the Earth's core, *Geomagn. Aeron.*, **4**, 572–583, English translation.
- Braginsky, S.I. & Roberts, P.H., 1995. Equations governing convection in Earth's core and the geodynamo, *Geophys. Astrophys. Fluid Dyn.*, **79**, 1–97.
- Chandrasekhar, S., 1961. *Hydrodynamic and Hydromagnetic Stability*, Clarendon Press.
- Dormy, E., Valet, J.-P. & Courtillot, V., 2000. Numerical models of the geodynamo and observational constraints, *Geochem. Geophys. Geosyst.*, **1**, doi:10.1029/2000GC0000062.
- Driscoll, P. & Olson, P., 2009. Effects of buoyancy and rotation on the polarity reversal frequency of gravitationally driven numerical dynamos, *Geophys. J. Int.*, **178**, 1337–1350.
- Glatzmaier, G.A. & Roberts, P.H., 1995a. A three-dimensional convective dynamo solution with rotating and finitely conducting inner core and mantle, *Phys. Earth planet. Inter.*, **91**, 63–75.
- Glatzmaier, G.A. & Roberts, P.H., 1995b. A three-dimensional self-consistent computer simulation of a geomagnetic field reversal, *Nature*, **377**, 203–208.
- Glatzmaier, G.A., Coe, R.S., Hongre, L. & Roberts, P.H., 1999. The role of the Earth's mantle in controlling the frequency of geomagnetic reversals, *Nature*, **401**, 885–890.
- Grote, E., Busse, F.H. & Tilgner, A., 2000. Regular and chaotic spherical dynamos, *Phys. Earth planet. Inter.*, **117**, 259–272.
- Gubbins, D., 1999. The distinction between geomagnetic excursions and reversals, *Geophys. J. Int.*, **137**(1), 1–4.
- Katayama, J.S., Matsushima, J.M. & Honkura, Y., 1999. Some characteristics of magnetic field behavior in a model of MHD dynamo thermally driven in a rotating spherical shell, *Phys. Earth planet. Inter.*, **111**, 141–159.
- Kono, M. & Roberts, P.H., 2002. Recent geodynamo simulations and observations of the geomagnetic field, *Rev. Geophys.*, **40**, 4-1–4-53.
- Kutzner, C. & Christensen, U., 2002. From stable dipolar towards reversing numerical dynamos, *Phys. Earth planet. Inter.*, **131**, 29–45.
- Kutzner, C. & Christensen, U.R., 2004. Simulated geomagnetic reversals and preferred virtual geomagnetic pole paths, *Geophys. J. Int.*, **157**, 1105–1118.
- McFadden, P.L. & Merrill, R.T., 1995. Fundamental transitions of the geodynamo as suggested by paleomagnetic data, *Phys. Earth planet. Inter.*, **91**, 253–260.
- Merrill, R.T. & McFadden, P.L., 1999. Geomagnetic polarity transitions, *Rev. Geophys.*, **37**, 201–226.
- Moffatt, H.K., 1978. *Magnetic Field Generation in Electrically Conducting Fluids*, Cambridge Univ. Press.
- Nishikawa, N. & Kusano, K., 2008. Simulation study of symmetry-breaking instability and dipole field reversal in a rotating spherical shell dynamo, *Phys. Plasmas*, **15**, 082903, doi:10.1063/1.2959120.
- Olson, P. & Amit, H., 2014. Magnetic reversal frequency in dynamos with thermochemical convection, *Phys. Earth planet. Inter.*, **229**, 122–133.
- Olson, P. & Christensen, U., 2006. Dipole moment scaling for convection-driven planetary dynamos, *Earth planet. Sci. Lett.*, **250**(3–4), 561–571.

- Olson, P., Christensen, U. & Glatzmaier, G., 1999. Numerical modeling of the geodynamo: mechanisms of field generation and equilibration, *J. geophys. Res.*, **104**, 10 383–10 404.
- Olson, P., Driscoll, P. & Amit, H., 2009. Dipole collapse and reversal precursors in a numerical dynamo, *Phys. Earth planet. Inter.*, **173**, 121–140.
- Rotvig, J., 2009. An investigation of reversing numerical dynamos driven by either differential or volumetric heating, *Phys. Earth planet. Inter.*, **176**, 69–82.
- Sarson, G.R. & Jones, C.A., 1999. A convection driven geodynamo reversal model, *Phys. Earth planet. Inter.*, **111**, 3–20.
- Sreenivasan, B., 2009. On dynamo action produced by boundary thermal coupling, *Phys. Earth planet. Inter.*, **77**, 130–138.
- Sreenivasan, B., 2010. Modelling the geodynamo: progress and challenges, *Curr. Sci.*, **99**(12), 1739–1750.
- Sreenivasan, B. & Gubbins, D., 2008. Dynamos with weakly convecting outer layers: implications for core–mantle boundary interaction, *Geophys. astrophys. Fluid Dyn.*, **102**(4), 395–407.
- Sreenivasan, B. & Jones, C.A., 2006. The role of inertia in the evolution of spherical dynamos, *Geophys. J. Int.*, **164**, 467–476.
- Sreenivasan, B. & Jones, C.A., 2011. Helicity generation and subcritical behaviour in rapidly rotating dynamos, *J. Fluid Mech.*, **688**, 5–30.
- Starchenko, S. & Jones, C.A., 2002. Typical velocities and magnetic fields in planetary interiors, *Icarus*, **157**, 426–435.
- Takahashi, F., Matsushima, M. & Honkura, Y., 2005. Simulations of a quasi-Taylor state geomagnetic field including polarity reversals on the Earth simulator, *Science*, **309**, 459–461.
- Taylor, J.B., 1963. The magneto-hydrodynamics of a rotating fluid and the Earth's dynamo problem, *Proc. R. Soc. Lond.*, **274**, 274–283.
- Valet, J., Meynardier, L. & Guyodo, Y., 2005. Geomagnetic field strength and reversal rate over the past 2 Million years, *Nature*, **435**, 802–805.
- Wicht, J. & Olson, P., 2004. A detailed study of the polarity reversal mechanism in a numerical dynamo model, *Geochem. Geophys. Geosyst.*, **5**, Q03H10, doi:10.1029/2003GC000602.